PHOTONICS Research

CMOS-compatible all-optical modulator based on the saturable absorption of graphene

Hong Wang,[1] Ningning Yang,[1] Limin Chang,[2] Chaobiao Zhou,[1] Shiyu Li,[1] Meng Deng,[1] Zhenwei Li,[1] Qiang Liu,[1] Chi Zhang,[1,3] Zhiyong Li,[2,4] and Yi Wang[1,*]

[1]Wuhan National Laboratory for Optoelectronics, Huazhong University of Science and Technology, Wuhan 430074, China
[2]Institute of Semiconductors, Chinese Academy of Sciences, Beijing 100038, China
[3]e-mail: chizheung@hust.edu.cn
[4]e-mail: lizhy@semi.ac.cn
*Corresponding author: ywangwnlo@hust.edu.cn

Received 11 October 2019; revised 14 January 2020; accepted 16 January 2020; posted 16 January 2020 (Doc. ID 380170); published 18 March 2020

Graphene resting on a silicon-on-insulator platform offers great potential for optoelectronic devices. In the paper, we demonstrate all-optical modulation on the graphene–silicon hybrid waveguides (GSHWs) with tens of micrometers in length. Owing to strong interaction between graphene and silicon strip waveguides with compact light confinement, the modulation depth reaches 22.7% with a saturation threshold down to 1.38 pJ per pulse and a 30-μm-long graphene pad. A response time of 1.65 ps is verified by a pump–probe measurement with an energy consumption of 2.1 pJ. The complementary metal-oxide semiconductor compatible GSHWs with the strip configuration exhibit great potential for ultrafast and broadband all-optical modulation, indicating that employing two-dimensional materials has become a complementary technology to promote the silicon photonic platform.

https://doi.org/10.1364/PRJ.380170

1. INTRODUCTION

Graphene, with a variety of exceptional electronic and photonic properties, has intrigued great research interests [1,2]. Photonic devices based on properties of graphene include mode-locked ultrafast lasers [3,4], optical modulators [5,6], and photodetectors [7–11], etc. Among them, optical modulators play a crucial role in optical interconnects. Benefiting from the Pauli blocking principle of graphene, the Fermi level of graphene can be modulated by electric gating [5] or optical excitation [12–30], which has been investigated to realize optical modulators. For graphene electro-optical modulators, the current modulation rate has reached tens of gigahertz by means of optimizing the device structures [31]. At present, the main bottleneck of electro-optic modulation is the resistor-capacitor effect [5,31]. Nevertheless, all-optical modulators can circumvent the limit by light pumping [32]. There have been some works about all-optical modulation based on the saturable absorption (SA) and Kerr effect of graphene on the fiber platform [12–15,17,26]. Attributed to the ultrafast carrier relaxation of graphene, the response times of devices based on the SA of graphene had reached picosecond scale on the fiber platform [6,14,33].

The fabrication process of graphene-assisted all-fiber is incompatible with the complementary metal-oxide semiconductor (CMOS) process, limiting their utilization in chip-scale optical interconnects. The silicon-on-insulator (SOI) platform is compact and compatible with CMOS [34,35], which is beneficial for integration and industrialization of all-optical modulators based on graphene. Nevertheless, limited by the intrinsic carrier lifetime of the silicon waveguides, all-optical modulators of silicon waveguides always have a long response time of hundreds of picoseconds [32]. Introducing the graphene samples with extraordinary optoelectronic characteristics to the SOI platform strengthens the non-linear susceptibility of silicon, leading to a lower power consumption, faster response, and larger integrated density. Compared with all-optical graphene modulators of fiber, there are fewer experimental works of all-optical modulation on silicon waveguides [20–23,25,36].

In this work, we transfer graphene onto silicon waveguides to form graphene–silicon hybrid waveguides (GSHWs). The SA of graphene is used to achieve all-optical modulation of GSHWs. We measure the SA of GSHWs with 500-nm-wide waveguides and 30-μm-long graphene pads, and the modulation depth (MD) reaches 22.7% with a saturation threshold down to 1.38 pJ per pulse. A pump–probe setup is employed and a response time of 1.65 ps is measured with an energy consumption of 2.1 pJ.

2. THEORETICAL MODEL AND SIMULATION RESULTS

The schematic of the GSHWs is illustrated in Fig. 1, which consists of a graphene pad, photonic crystal gratings, and a strip waveguide on the SOI platform. For GSHWs, the MD can be manipulated by the interaction between the evanescent field and graphene, which depends on the parameters as follows.

When $\hbar\omega$ and $|\mu_c| \gg k_B T$, the surface dynamic conductivity of graphene can be treated in a complex form consisting of interband and intraband contributions [37–39], which can be expressed by the following formula:

$$\sigma(\omega,\mu_c,\tau,t) = i\frac{e^2 k_B t}{\pi\hbar^2(\omega + i\tau^{-1})}\left[\frac{|\mu_c|}{k_B t} + 2\ln\left(e^{-\frac{|\mu_c|}{k_B t}} + 1\right)\right] + i\frac{e^2}{4\pi\hbar}\ln\left[\frac{2|\mu_c| - \hbar(\omega + i\tau^{-1})}{2|\mu_c| + \hbar(\omega + i\tau^{-1})}\right], \quad (1)$$

where e is the electron charge, k_B is the Boltzmann constant, $\hbar$ is the reduced Planck's constant, ω is the angular frequency of the incident light, t is the temperature, μ_c is the chemical potential, and τ is the momentum relaxation of carriers in monolayer graphene. In Fig. 2(a), $\sigma(\omega,\mu_c,\tau,t)$ is numerically calculated and plotted as a function of graphene's chemical potential at $t = 300$ K, $\tau = 12$ fs with the incident light of 1550 nm. The value of τ has been observed in recent experiments [40,41]. When the Fermi level is about 0.4 eV, the conductivity of the GSHWs changes sharply, implying a sharp decrease in the linear loss of waveguides, owing to the principle of Pauli blocking. When the Fermi level is away from half of the energy of incident light, the optical linear absorption is not sensitive to chemical potential and incident wavelengths. Figure 2(b) shows the variation of σ as a function of the wavelength of incident light at the Fermi level of 0.4 eV. The optical linear absorption coefficient (LAC) of graphene is directly determined by the real part of its surface dynamic conductivity, i.e., the imaginary part of permittivity.

When electric fields are perpendicular to the surface of waveguides (x–y plane), the corresponding surface current density could be neglected owing to non-interaction between graphene and waveguides. The surface current density of monolayer graphene is expressed as [42,43]

$$\mathbf{J}_{//} = \sigma(\omega,\mu_c,\tau,t)\mathbf{E}_{//}, \quad (2)$$

$$\mathbf{J}_{\perp} = 0, \quad (3)$$

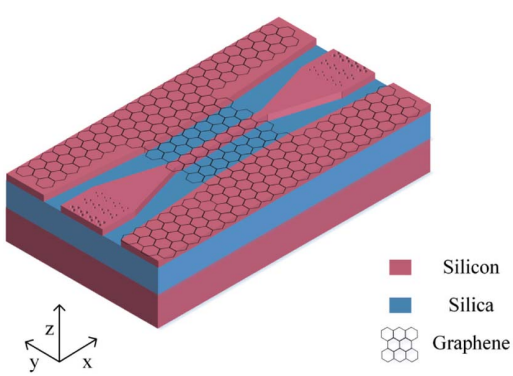

Fig. 1. Schematic of GSHWs consisting of a graphene pad, a strip waveguide, and photonic crystal gratings.

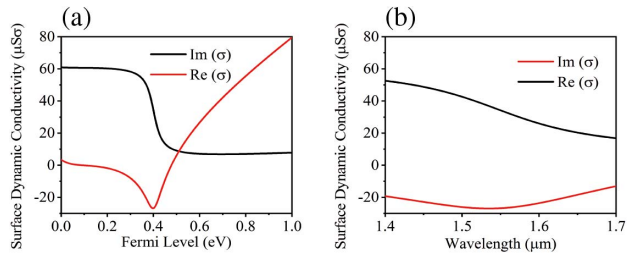

Fig. 2. Surface dynamic conductivity of monolayer graphene versus its (a) chemical potential and (b) wavelength of incident light.

where subscripts // and ⊥ denote the field components which are tangential and normal to the graphene sheet, respectively. **E** is the electrical field and **J** is the surface current density of monolayer graphene. Figures 3(a) and 3(b) represent the real and imaginary parts of the effective refractive index (ERI) of a GSHW composing of 500-nm width and 220-nm height, which is pumped by a 1550-nm incident light with Fermi levels ranging from 0.12 to 0.6 eV for transverse electric (TE) and transverse magnetic (TM) modes, respectively. Here, all simulations are calculated in COMSOL Multiphysics. Mesh grids are presented in our previous work (Ref. [37]). The tendency of the ERI is in accordance with the one of σ as a function of Fermi levels, which implies that the changeable ERI of GSHWs through controlling the Fermi level of graphene is expected in application of optical modulation.

The LAC (i.e., the linear limit of the SA [44]) of the in-plane monolayer graphene is obtained through [45]

$$\alpha_s(\mu\text{m}^{-1}) = 2k_0 n_{\text{eff,imag}} \times 10^{-6}, \quad (4)$$

where k_0 is the vacuum wavenumber, and subscript "imag" denotes the imaginary part of the ERI. The LAC is shown in Fig. 3(c) for TE and TM modes, respectively. As the two-level saturable absorber model is widely used in two-dimensional quantum wells, the absorption as a function of the light intensity can be fitted by $\alpha(I) = \alpha_s/(1 + I/I_s) + \alpha_{ns}$, where I_s is the threshold intensity of the SA, defined as the optical intensity required in a steady state to reduce the absorption to half of the unbleached value, and α_{ns} is the non-saturable absorption coefficient mainly determined by the scattering loss of graphene [3]. When the light intensity is high enough, the absorption coefficient of graphene is close to α_{ns}. Finally, the MD is given by [44,46,47]

$$\begin{aligned}\frac{\Delta T}{T_o} &= \frac{T_{ns} - T_o}{T_o} \times 100\% \\ &= \frac{e^{-\alpha_{ns}L} - e^{-\alpha L}}{e^{-\alpha L}} \times 100\% \\ &= (e^{\alpha_s L} - 1) \times 100\%,\end{aligned} \quad (5)$$

where L is the length of graphene, and α is the absorption coefficient of graphene mainly resulting from the interband transition of carriers and the scattering of graphene coming from the residual aggregates, contamination, wrinkles, and cracks [3,12,15].

Moreover, we simulate the dependence of the MD on wavelengths of incident light, Fermi levels, dimensions of GSHWs,

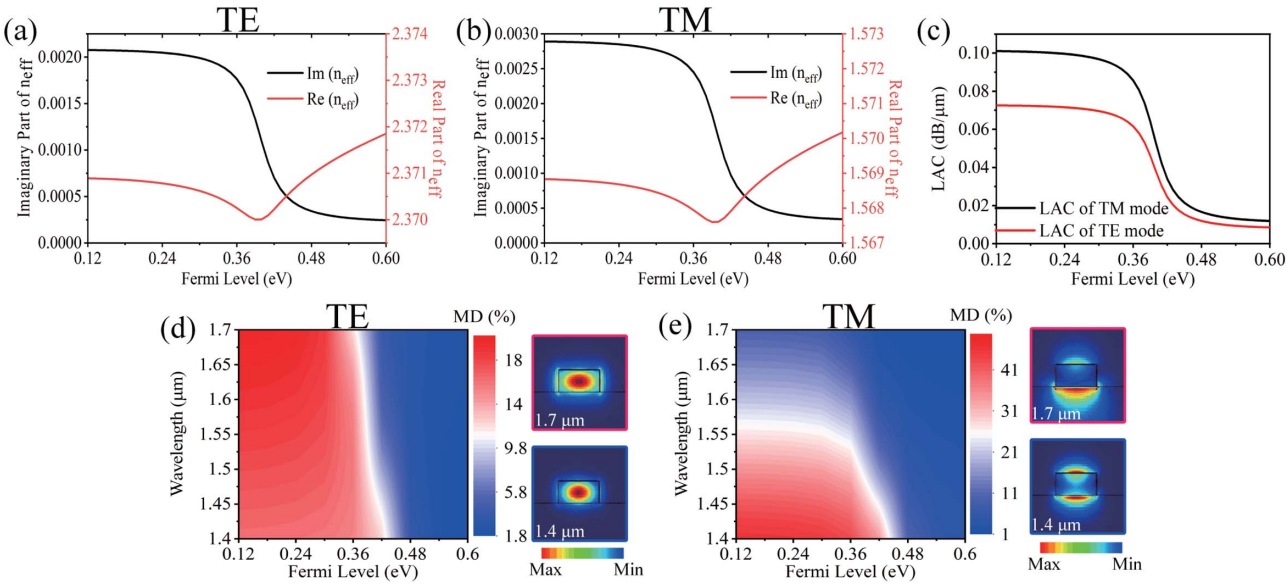

Fig. 3. (a)–(c) Real and imaginary parts of ERI and LAC at 500-nm width, 220-nm height, and 1550-nm wavelength with Fermi levels ranging from 0.12 eV to 0.6 eV for TE and TM modes, respectively. (d) The MDs are calculated with 10-μm-long graphene (the insets are electric field profiles of the TE mode at 1.4 and 1.7 μm wavelengths, respectively). (e) The MDs for TM mode under the same conditions.

and lengths of graphene pads. Figures 3(d) and 3(e) depict the dependence of the MD on wavelengths of incident light and Fermi levels of graphene for TE and TM modes, respectively. The GSHW with a width of 500 nm, a height of 220 nm, and a 10-μm-long graphene pad is pumped by a 1550-nm input light. As shown in Fig. 3(d), the larger values of the MD are achieved with longer incident wavelengths because stronger light–matter interaction is obtained by the longer incident wavelength, in comparison to that obtained by the shorter incident wavelength shown in the inset. Also lower doping level of graphene is also preferred owing to the larger absorption of graphene. As the TM mode is shown in Fig. 3(e), the increment of the MD over 2.5 times is obtained with shorter wavelengths because of the strengthened leaky field on top of the silicon waveguides, compared to the TE mode. The dependence of the MDs on Fermi levels implies that the values of the MDs can be changed through electronic doping and optical exciters.

As shown in Figs. 4(a) and 4(b), we also calculate the dependence of the MD on the widths and heights of GSHWs for the TE and TM modes with a 10-μm-long graphene pad and the incident wavelength is 1550 nm at the Fermi level of 0.4 eV. For the TE mode, the MD reduces with the increment of the width and height, since less light can be evanescently coupled into the graphene. The change of the MD is more sensitive to the variation of the height of waveguides than the variation of the width of waveguides. Nevertheless, the MDs of the TM mode have a peak value with a height about 250 nm and a width of 600 nm. For smaller values of width, the value of height with peak MD is greater. We further simulate the dependence of the MD on the length of graphene with 500-nm-wide waveguides and a Fermi level of 0.4 eV at 1550 nm, which exhibits a clear exponential trend in Fig. 4(c) as described by Eq. (5).

3. EXPERIMENTS

A. Sample Preparation

Here, we perform an experimental demonstration of the all-optical modulation based on GSHWs. The thicknesses of the

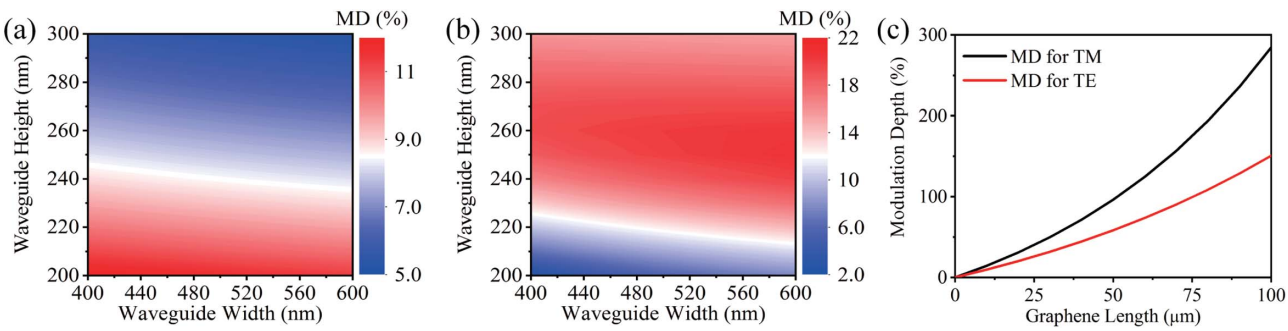

Fig. 4. (a), (b) Simulated MDs depending on the width and height of GSHWs with the Fermi level of 0.4 eV and 10-μm-long graphene pad for the TE and TM modes, respectively. (c) The dependence of MDs on the different lengths of graphene for the TE and TM modes with the 500-nm-wide waveguide and Fermi level of 0.4 eV.

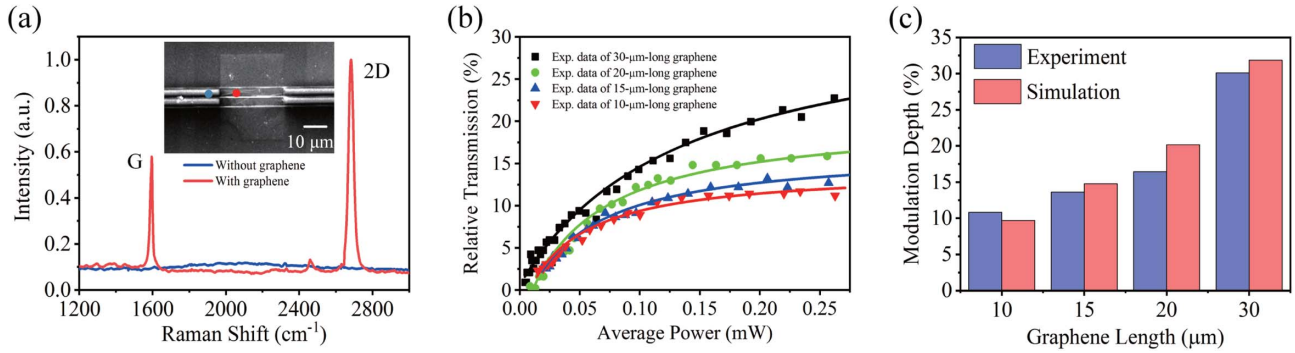

Fig. 5. (a) Raman spectra of the GSHWs (the inset figure is the SEM picture of graphene pad, the blue circle represents the spot where graphene is etched off, the red circle represents the spot where graphene is protected). (b) The experimental transmission data and fitted curves as a function of input power for the TE mode. Here, the relative transmission is expressed as $\frac{T-T_o}{T_o} \times 100\%$. (c) The comparison of MDs in simulated and experimental results with 10-, 15-, 20-, and 30-μm-long graphene pads (the GSHW with 30-μm-long graphene is not saturated sufficiently with the maximum power of the femtosecond laser we use. Here, we use the fitted MD of 30.1% from the measured data).

top silicon layer and the buried oxide layer are 220 nm and 2 μm, respectively. The silicon waveguides supporting the TE mode consist of 500-nm-wide strip waveguides as well as input and output photonic crystal grating couplers exhibiting an insertion loss of ~7.5 dB per facet at about 1560 nm. The electron-beam lithography (EBL) is used for mask formation and inductively coupled plasma is used for etching silicon with sulfur hexafluoride gas. Then, a monolayer graphene sheet (Hefei Vigon Co., Ltd.) grown by chemical vapor deposition (CVD) is transferred onto the silicon waveguide by the wet-transferring method [37,48], which is depicted as follows. (i) The graphene film with polymer (polymethyl methacrylate, PMMA) on the top and copper foil on the bottom is floated on the etchant with 10 g of copper (II) sulfate pentahydrate ($CuSO_4 \cdot 5H_2O$), 50 mL of de-ionized (DI) water, and 50 mL of concentrated hydrochloric acid (HCl). (ii) After an etching time of about an hour, the PMMA/graphene film without Cu is transferred into a clean beaker and cleaned with DI water. (iii) The chip is dipped into DI water to scoop up the floated PMMA/graphene. Then the sample bakes for 20 min to melt the PMMA resist for better contact between the graphene and waveguides. (iv) We put the chip into acetone for 10–15 min to remove the PMMA. In order to precisely control the MD of the GSHWs, the PMMA layer is coated on graphene and patterned by EBL. The redundant graphene layer is etched off through reactive ion etching (RIE) using oxygen, leaving graphene pads with tens of micrometers length on strip waveguides. The image taken by scanning electron microscopy (SEM) [inset of Fig. 5(a)] of a GSHW shows a graphene pad resting on the top of a silicon strip waveguide. Owing to the large conductivity difference between the graphene and the substrate, the shape of the graphene pad can be clearly seen.

B. SA of the GSHWs

Figure 5(a) exhibits the Raman spectra of the graphene pad which are acquired by a LabRAM HR800 with 532-nm excitation. The red curve shows a G peak (1595 cm^{-1}) with a full width at half-maximum (FWHM) of 10 cm^{-1}, a 2D peak (2683 cm^{-1}) with a 2D-to-G peak intensity ratio of about 1.6, and an inconspicuous D peak, implying the good quality of the transferred monolayer graphene with a Fermi level of about −0.4 eV [49]. The blue curve shows no characteristic peaks of graphene, indicating the graphene is etched off effectively by RIE.

The LACs of the GSHWs are characterized by a cutoff method and the measured result is about 0.049 dB/μm, which is close to the simulated result (0.039 dB/μm). The error may come from the scattering loss of the graphene resulting from the process of CVD growth and transfer of graphene. A homemade femtosecond fiber laser with a center wavelength of 1560 nm (pulse width: ~900 fs, repetition rate: 92.9 MHz) is coupled into the GSHWs as a pump source. Four GSHWs with increasing lengths of graphene pads are applied for the SA measurement. The input light strongly interacts with graphene through evanescent coupling owing to the tight bonding between strip waveguides and graphene pads. As the intensity of light increases, the photogenerated carriers lead to the fulfillment of the states near the edge of the conduction and valence bands of graphene [3]. The SA or bleaching of incident light is achieved, resulting in a higher transmission of GSHWs.

As shown in the red triangles in Fig. 5(b), for the GSHW with a 10-μm-long graphene pad, the transmission increases nonlinearly with rising input power. The averaged threshold power of the SA is 0.043 mW, corresponding to a threshold of 0.47 W in peak power (i.e., pulse energy of 423 fJ). For the compact silicon waveguide with an effective mode area of 1.02×10^{-9} cm^2, the peak power density arrives at 0.46 GW/cm^2. In addition, the MDs of 500-nm-wide waveguides with 15-, 20-, and 30-μm graphene pads are also provided in blue triangles, green circles, and black squares in Fig. 5(b), exhibiting MDs of 13.6%, 16.4%, and 22.7% with the threshold powers of 0.054, 0.065, and 0.14 mW (i.e., pulse energies of 532, 641, and 1380 fJ), respectively. It is noted that the 30-μm-long graphene pad is not saturated sufficiently with the maximum power of the femtosecond laser we have (the MD can reach 30.1% according to the fitted data). The simulated results (9.7%, 13.6%, 16.4%, and 31.9%) from Fig. 4(c) are in good agreement with the experimental results from Fig. 5(b), which is shown in Fig. 5(c).

Here, the modulation efficiency, defined as the MD per unit length of the device, is about 0.033 dB/μm, which could be further approved by the enhancement of interaction between light and graphene [16,18]. Slot waveguides with smaller effective mode areas may improve modulation efficiency and reduce energy per pulse further [25]. Although the graphene pad with longer length increases the MD, more energy consumption is brought. In order to achieve enough MD and reasonable energy consumption, we choose GSHWs with 30-μm-long graphene in the following experiments of demonstration of all-optical modulation and the response time of the devices.

C. Demonstration of All-Optical Modulation of GSHWs and Response Time of Devices

To demonstrate the all-optical modulation of GSHWs, we built a measurement system shown in Fig. 6(a). The pump light at 1560 nm is modulated by an electro-optic modulator with a period of 1 kHz and a duty cycle of 0.1%. After passing through an erbium-doped fiber amplifier (EDFA) (labeled as EDFA 1), a successive bandpass filter (BPF) (labeled as BPF 1) allows 3-nm bandwidth ranging from 1558.5 to 1561.5 nm to pass. The filtered light couples into the GSHW (500-nm-wide waveguide with 30-μm-long graphene) from Port 2 of the coupler with an average power of 0.04 mW. The probe light at 1565 nm couples into the GSHW from Port 1 with an average power of 0.21 mW. After passing through the GSHW, the probe light is filtered out with a 1565 ± 1 nm BPF (labeled as BPF 2) and amplified by another EDFA (labeled as EDFA 2) to achieve enough intensity for the photodetector. Figure 6(b) displays the modulation of the probe light by the pump light, and Fig. 6(c) shows the temporal profile of a single pulse. With the CW signal beam in, the output light at 1565 nm appears in a form of spikes with a period of 1 ms synchronized with the repetition rate (1 kHz) of the modulating pulses. The modulation process shows the following scenario. The pump light excites carriers of graphene from the valence band to the conduction band through the evanescent coupling between the graphene pad and silicon waveguides. When the light intensity is strong enough, because of the Pauli blocking principle, the linear absorption of graphene is inhibited, resulting in an enhanced transmission of the probe light. Considering the ultrafast relaxation of graphene carriers, a response time of picosecond is expected [6,14,16,33]. Nevertheless, limed by the speed of electric-to-optical and optical-to-electric devices, optical pump–probe spectroscopy measurement should be employed.

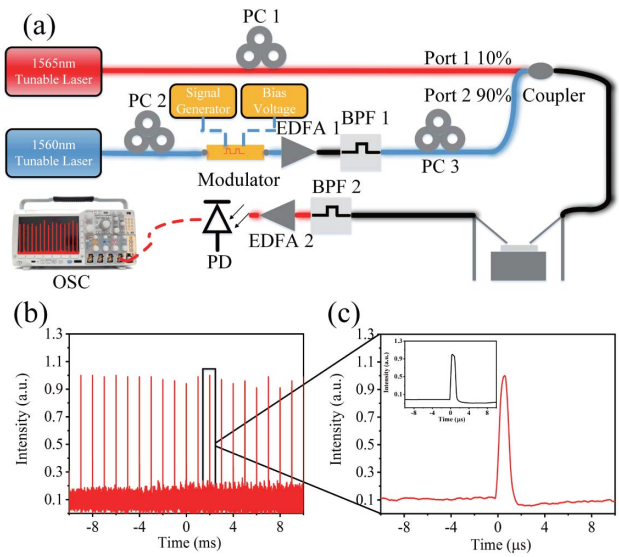

Fig. 6. (a) Schematic of the experimental system. (b) Time history of the modulated probe light with the pump light acquired by the oscilloscope (OSC). (c) Time profile of a probe pulse (the inset is the temporal profile of a pump pulse).

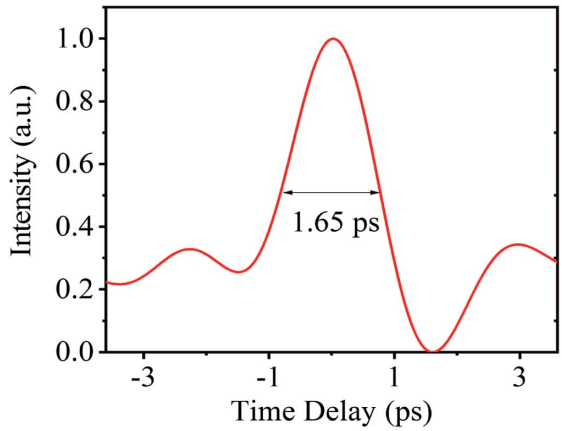

Fig. 7. Change in transmission of the probe light as a function of its time delay relative to the pump light. The FWHM is about 1.65 ps.

To explore the ultrafast response of GSHWs, we use an asynchronous pump–probe measurement which is stable, fast, and with a longer scan range compared with the conventional pump–probe spectroscopy setups using mechanical delay lines [50,51]. Here, the pump light (about 700 fs) is filtered from 1530 to 1560 nm with an average power of 0.19 mW (2.1 pJ per pulse). The average power of the probe light (about 300 fs) is 0.021 mW with a central wavelength of 1560 nm. As shown in Fig. 7, the temporal transmission of the probe light as a function of its time delay relative to the pump light is illustrated. The rise time of temporal transmission is about 1.2 ps, which is still limited by the resolution time of the asynchronous pump–probe system. Although the time resolution of 700 fs should be achieved, dispersion elements of the system, for example, the single-mode fibers, broaden the width of the pulse in the temporal domain. The FWHM is about 1.65 ps, corresponding to the bandwidth of about 500 GHz, which is in good agreement with the previous results [6,14,16,33].

4. CONCLUSION

In summary, an all-optical modulator has been realized by the GSHW. The modulation depth reached 22.7% with a saturation threshold down to 1.38 pJ per pulse with a 30-μm-long graphene pad. The MD can be manipulated by the dimension of waveguides, length, and the Fermi level of graphene through electronic doping and optical exciters. An ultrashort response time of 1.65 ps was obtained by a pump–probe measurement with 2.1 pJ per pulse. The all-optical modulator based on GSHW, with the combined advantages of a compact footprint,

broadband operation, the response time of few picoseconds, energy consumption of picojoule per pulse, and compatibility with CMOS, could bring us a step closer to realizing on-chip all-optical control.

Funding. National Natural Science Foundation of China (61775075); State Key Laboratory of Advanced Optical Communication Systems and Networks, Shanghai Jiao Tong University, China (2019GZKF03005).

Acknowledgment. We thank all engineers in the Center of Micro-Fabrication and Characterization (CMFC) of Wuhan National Laboratory for Optoelectronics (WNLO) for the support in fabrication.

Disclosures. The authors declare no conflicts of interest.

REFERENCES

1. F. Bonaccorso, Z. Sun, T. Hasan, and A. C. Ferrari, "Graphene photonics and optoelectronics," Nat. Photonics **4**, 611–622 (2010).
2. Q. Bao and K. P. Loh, "Graphene photonics, plasmonics, and broadband optoelectronic devices," ACS Nano **6**, 3677–3694 (2012).
3. Q. Bao, Z. Han, W. Yu, Z. Ni, Y. Yan, Z. X. Shen, K. P. Loh, and Y. T. Ding, "Atomic-layer graphene as a saturable absorber for ultrafast pulsed lasers," Adv. Funct. Mater. **19**, 3077–3083 (2010).
4. Z. Sun, T. Hasan, F. Torrisi, D. Popa, G. Privitera, F. Wang, F. Bonaccorso, D. M. Basko, and A. C. Ferrari, "Graphene mode-locked ultrafast laser," ACS Nano **4**, 803–810 (2010).
5. M. Liu, X. Yin, E. Ulin-Avila, B. Geng, T. Zentgraf, L. Ju, F. Wang, and X. Zhang, "A graphene-based broadband optical modulator," Nature **474**, 64–67 (2011).
6. W. Li, B. Chen, C. Meng, W. Fang, Y. Xiao, X. Li, Z. Hu, Y. Xu, L. Tong, H. Wang, W. Liu, J. Bao, and Y. R. Shen, "Ultrafast all-optical graphene modulator," Nano Lett. **14**, 955–959 (2014).
7. Z. Sun and H. Chang, "Graphene and graphene-like two-dimensional materials in photodetection: mechanisms and methodology," ACS Nano **8**, 4133–4156 (2014).
8. F. Xia, T. Mueller, Y.-M. Lin, A. Valdes-Garcia, and P. Avouris, "Ultrafast graphene photodetector," Nat. Nanotechnol. **4**, 839–843 (2009).
9. X. Gan, R.-J. Shiue, Y. Gao, I. Meric, T. F. Heinz, K. Shepard, J. Hone, S. Assefa, and D. Englund, "Chip-integrated ultrafast graphene photodetector with high responsivity," Nat. Photonics **7**, 883–887 (2013).
10. X. Wang, Z. Cheng, K. Xu, H. K. Tsang, and J.-B. Xu, "High-responsivity graphene/silicon-heterostructure waveguide photodetectors," Nat. Photonics **7**, 888–891 (2013).
11. T. Yang, H. Lin, and B. Jia, "Two-dimensional material functional devices enabled by direct laser fabrication," Front. Optoelectron. **11**, 2–22 (2017).
12. X. Wu, S. Yu, H. Yang, W. Li, X. Liu, and L. Tong, "Effective transfer of micron-size graphene to microfibers for photonic applications," Carbon **96**, 1114–1119 (2016).
13. Z. B. Liu, M. Feng, W. S. Jiang, W. Xin, P. Wang, Q. W. Sheng, Y. G. Liu, D. N. Wang, W. Y. Zhou, and J. G. Tian, "Broadband all-optical modulation using a graphene-covered-microfiber," Laser Phys. Lett. **10**, 065901 (2013).
14. S. Yu, C. Meng, B. Chen, H. Wang, X. Wu, W. Liu, S. Zhang, Y. Liu, Y. Su, and L. Tong, "Graphene decorated microfiber for ultrafast optical modulation," Opt. Express **23**, 10764–10770 (2015).
15. S. Yu, X. Wu, K. Chen, B. Chen, X. Guo, D. Dai, L. Tong, W. Liu, and Y. R. Shen, "All-optical graphene modulator based on optical Kerr phase shift," Optica **3**, 541–544 (2016).
16. H. Zhang, N. Healy, L. Shen, C. C. Huang, D. W. Hewak, and A. C. Peacock, "Enhanced all-optical modulation in a graphene-coated fibre with low insertion loss," Sci. Rep. **6**, 23512 (2016).
17. R. Wang, D. Li, H. Wu, M. Jiang, Z. Sun, Y. Tian, J. Bai, and Z. Ren, "All-optical intensity modulator by polarization-dependent graphene-microfiber waveguide," IEEE Photonics J. **9**, 7105708 (2017).
18. C. Meng, S.-L. Yu, H.-Q. Wang, Y. Cao, L.-M. Tong, W.-T. Liu, and Y.-R. Shen, "Graphene-doped polymer nanofibers for low-threshold nonlinear optical waveguiding," Light Sci. Appl. **4**, e348 (2015).
19. X. Gan, C. Zhao, Y. Wang, D. Mao, L. Fang, L. Han, and J. Zhao, "Graphene-assisted all-fiber phase shifter and switching," Optica **2**, 468–471 (2015).
20. Z. Jafari, A. Zarifkar, M. Miri, and L. Zhang, "All-optical modulation in a graphene-covered slotted silicon nano-beam cavity," J. Lightwave Technol. **36**, 4051–4059 (2018).
21. K. J. A. Ooi, P. C. Leong, L. K. Ang, and D. T. H. Tan, "All-optical control on a graphene-on-silicon waveguide modulator," Sci. Rep. **7**, 12748 (2017).
22. K.-J. Peng, C.-L. Wu, Y.-H. Lin, H.-Y. Wang, C.-H. Cheng, Y.-C. Chi, and G.-R. Lin, "Saturated evanescent-wave absorption of few-layer graphene-covered side-polished single-mode fiber for all-optical switching," Nanophotonics **7**, 207–215 (2018).
23. Z. Shi, L. Gan, T.-H. Xiao, H.-L. Guo, and Z.-Y. Li, "All-optical modulation of a graphene-cladded silicon photonic crystal cavity," ACS Photonics **2**, 1513–1518 (2015).
24. F. Sun, L. Xia, C. Nie, J. Shen, Y. Zou, G. Cheng, H. Wu, Y. Zhang, D. Wei, S. Yin, and C. Du, "The all-optical modulator in dielectric-loaded waveguide with graphene-silicon heterojunction structure," Nanotechnology **29**, 135201 (2018).
25. F. Sun, L. Xia, C. Nie, C. Qiu, L. Tang, J. Shen, T. Sun, L. Yu, P. Wu, S. Yin, S. Yan, and C. Du, "An all-optical modulator based on a graphene-plasmonic slot waveguide at 1550 nm," Appl. Phys. Express **12**, 042009 (2019).
26. R. Wang, D. Li, M. Jiang, H. Wu, X. Xu, and Z. Ren, "All-optical intensity modulation based on graphene-coated microfibre waveguides," Opt. Commun. **410**, 604–608 (2018).
27. P. Weis, J. L. Garcia-Pomar, M. Hoh, B. Reinhard, A. Brodyanski, and M. Rahm, "Spectrally wide-band terahertz wave modulator based on optically tuned graphene," ACS Nano **6**, 9118–9124 (2012).
28. Q. Y. Wen, W. Tian, Q. Mao, Z. Chen, W. W. Liu, Q. H. Yang, M. Sanderson, and H. W. Zhang, "Graphene based all-optical spatial terahertz modulator," Sci. Rep. **4**, 7409 (2014).
29. L. Yu, J. Zheng, Y. Xu, D. Dai, and S. He, "Local and nonlocal optically induced transparency effects in graphene-silicon hybrid nanophotonic integrated circuits," ACS Nano **8**, 11386–11393 (2014).
30. F. Zhou and W. Du, "Ultrafast all-optical plasmonic graphene modulator," Appl. Opt. **57**, 6645–6650 (2018).
31. V. Sorianello, M. Midrio, G. Contestabile, I. Asselberghs, J. Van Campenhout, C. Huyghebaert, I. Goykhman, A. K. Ott, A. C. Ferrari, and M. Romagnoli, "Graphene-silicon phase modulators with gigahertz bandwidth," Nat. Photonics **12**, 40–44 (2017).
32. Z. Chai, X. Hu, F. Wang, X. Niu, J. Xie, and Q. Gong, "Ultrafast all-optical switching," Adv. Opt. Mater. **5**, 1600665 (2017).
33. M. Ono, M. Hata, M. Tsunekawa, K. Nozaki, H. Sumikura, and M. Notomi, "Ultrafast and energy-efficient all-optical modulator based on deep-subwavelength graphene-loaded plasmonic waveguides," in *Conference on Lasers & Electro-Optics (CLEO)* (OSA, 2018), paper FF2L.4.
34. L. Thylén and L. Wosinski, "Integrated photonics in the 21st century," Photon. Res. **2**, 75–81 (2014).
35. Z. Zhou, B. Yin, Q. Deng, X. Li, and J. Cui, "Lowering the energy consumption in silicon photonic devices and systems [invited]," Photon. Res. **3**, B28–B46 (2015).
36. M. Ono, M. Hata, M. Tsunekawa, K. Nozaki, H. Sumikura, H. Chiba, and M. Notomi, "Ultrafast and energy-efficient all-optical switching with graphene-loaded deep-subwavelength plasmonic waveguides," Nat. Photonics **14**, 37–43 (2020).
37. H. Cai, Y. Cheng, H. Zhang, Q. Huang, J. Xia, R. Barille, and Y. Wang, "Enhanced linear absorption coefficient of in-plane monolayer graphene on a silicon microring resonator," Opt. Express **24**, 24105–24116 (2016).
38. P.-Y. Chen and A. Alù, "Atomically thin surface cloak using graphene monolayers," ACS Nano **5**, 5855–5863 (2011).

39. L. A. Falkovsky, S. S. Pershoguba, L. A. Falkovsky, and S. S. Pershoguba, "Optical far-infrared properties of a graphene monolayer and multilayer," Phys. Rev. B **76**, 153410 (2007).
40. Y. W. Tan, Y. Zhang, K. Bolotin, Y. Zhao, S. Adam, E. H. Hwang, S. Das Sarma, H. L. Stormer, and P. Kim, "Measurement of scattering rate and minimum conductivity in graphene," Phys. Rev. Lett. **99**, 246803 (2007).
41. Y.-C. Chang, C.-H. Liu, C.-H. Liu, Z. Zhong, and T. B. Norris, "Extracting the complex optical conductivity of mono- and bilayer graphene by ellipsometry," Appl. Phys. Lett. **104**, 261909 (2014).
42. G. Kovacevic and S. Yamashita, "Waveguide design parameters impact on absorption in graphene coated silicon photonic integrated circuits," Opt. Express **24**, 3584–3591 (2016).
43. D. Chatzidimitriou, A. Pitilakis, and E. E. Kriezis, "Rigorous calculation of nonlinear parameters in graphene-comprising waveguides," J. Appl. Phys. **118**, 023105 (2015).
44. V. Scardaci, Z. Sun, F. Wang, A. G. Rozhin, T. Hasan, F. Hennrich, I. H. White, W. I. Milne, and A. C. Ferrari, "Carbon nanotube polycarbonate composites for ultrafast lasers," Adv. Mater. **20**, 4040–4043 (2008).
45. Y. Ding, X. Zhu, S. Xiao, H. Hu, L. H. Frandsen, N. A. Mortensen, and K. Yvind, "Effective electro-optical modulation with high extinction ratio by a graphene-silicon microring resonator," Nano Lett. **15**, 4393–4400 (2015).
46. Y. Yang, Z. Xu, X. Jiang, Y. He, X. Guo, Y. Zhang, C. Qiu, and Y. Su, "High-efficiency and broadband four-wave mixing in a silicon-graphene strip waveguide with a windowed silica top layer," Photon. Res. **6**, 965–970 (2018).
47. J. Wang, L. Zhang, Y. Chen, Y. Geng, X. Hong, X. Li, and Z. Cheng, "Saturable absorption in graphene-on-waveguide devices," Appl. Phys. Express **12**, 032003 (2019).
48. C. Zhou, G. Liu, G. Ban, S. Li, Q. Huang, J. Xia, Y. Wang, and M. Zhan, "Tunable Fano resonator using multilayer graphene in the near-infrared region," Appl. Phys. Lett. **112**, 101904 (2018).
49. A. Das, S. Pisana, B. Chakraborty, S. Piscanec, S. K. Saha, U. V. Waghmare, K. S. Novoselov, H. R. Krishnamurthy, A. K. Geim, A. C. Ferrari, and A. K. Sood, "Monitoring dopants by Raman scattering in an electrochemically top-gated graphene transistor," Nat. Nanotechnol. **3**, 210–215 (2008).
50. S. A. Claussen, E. Tasyurek, J. E. Roth, and D. A. B. Miller, "Measurement and modeling of ultrafast carrier dynamics and transport in germanium/silicon-germanium quantum wells," Opt. Express **18**, 25596–25607 (2010).
51. X. Zhao, Z. Zheng, L. Liu, Q. Wang, H. Chen, and J. Liu, "Fast, long-scan-range pump-probe measurement based on asynchronous sampling using a dual-wavelength mode-locked fiber laser," Opt. Express **20**, 25584–25589 (2012).